Partitioning of discrete proton arcs into interlaced subplans can bring proton arc advances to existing proton facilities

Engwall, Erik; Marthin, Otte; Wase, Viktor; Sundström, Johan; Mikhalev, Victor; de Jong, Bas A.; Langendijk, Johannes A.; Melbéus, Henrik; Andersson, Björn; Korevaar, Erik W.

Published in:
Medical Physics

DOI:
10.1002/mp.16617

Publication date:
2023

Received: 27 April 2023 | Accepted: 19 June 2023

DOI: 10.1002/mp.16617

RESEARCH ARTICLE

MEDICAL PHYSICS

Partitioning of discrete proton arcs into interlaced subplans can bring proton arc advances to existing proton facilities

Erik Engwall[1] | **Otte Marthin**[1] | **Viktor Wase**[1] | **Johan Sundström**[1] | **Victor Mikhalev**[1] | **Bas A. de Jong**[2] | **Johannes A. Langendijk**[2] | **Henrik Melbéus**[1] | **Björn Andersson**[1] | **Erik W. Korevaar**[2] | **Stefan Both**[2] | **Rasmus Bokrantz**[1] | **Lars Glimelius**[1] | **Albin Fredriksson**[1]

[1]RaySearch Laboratories, Stockholm, Sweden

[2]Department of Radiation Oncology, University Medical Center Groningen, University of Groningen, Groningen, The Netherlands

Correspondence
Erik Engwall, RaySearch Laboratories, Stockholm, Sweden.
Email: erik.engwall@raysearchlabs.com

Abstract

Background: Proton arcs have shown potential to reduce the dose to organs at risks (OARs) by delivering the protons from many different directions. While most previous studies have been focused on dynamic arcs (delivery during rotation), an alternative approach is discrete arcs, where step-and-shoot delivery is used over a large number of beam directions. The major advantage of discrete arcs is that they can be delivered at existing proton facilities. However, this advantage comes at the expense of longer treatment times.

Purpose: To exploit the dosimetric advantages of proton arcs, while achieving reasonable delivery times, we propose a partitioning approach where discrete arc plans are split into subplans to be delivered over different fractions in the treatment course.

Methods: For three oropharyngeal cancer patients, four different arc plans have been created and compared to the corresponding clinical IMPT plan. The treatment plans are all planned to be delivered in 35 fractions, but with different delivery approaches over the fractions. The first arc plan (1×30) has 30 directions to be delivered every fraction, while the others are partitioned into subplans with 10 and 6 beam directions, each to be delivered every third (3×10), fifth fraction (5×6), or seventh fraction (7×10). All plans are assessed with respect to delivery time, target robustness over the treatment course, doses to OARs and NTCP for dysphagia and xerostomia.

Results: The delivery time (including an additional delay of 30 s between the discrete directions to simulate manual interaction with the treatment control system) is reduced from on average 25.2 min for the 1×30 plan to 9.2 min for the 3×10 and 7×10 plans and 5.7 min for the 5×6 plans. The delivery time for the IMPT plan is 7.9 min. When accounting for the combination of delivery time, target robustness, OAR sparing, and NTCP reduction, the plans with 10 directions in each fraction are the preferred choice. Both the 3×10 and 7×10 plans show improved target robustness compared to the 1×30 plans, while keeping OAR doses and NTCP values at almost as low levels as for the 1×30 plans. For all patients the NTCP values for dysphagia are lower for the partitioned plans with 10 directions compared to the IMPT plans. NTCP reduction for xerostomia compared to IMPT is seen in two of the three patients. The best results are seen for the first patient, where the NTCP reductions for the 7×10 plan are 1.6 p.p. (grade 2 xerostomia) and 1.5 p.p. (grade 2 dysphagia). The

corresponding NTCP reductions for the 1×30 plan are 2.7 p.p. (xerostomia, grade 2) and 2.0 p.p. (dysphagia, grade 2).
Conclusions: Discrete proton arcs can be implemented at any proton facility with reasonable treatment times using a partitioning approach. The technique also makes the proton arc treatments more robust to changes in the patient anatomy.

KEYWORDS
discrete arc, pencil-beam scanning, proton arc, proton planning, static arc

1 | INTRODUCTION

During the past years, proton arc treatment has sparked increasing attention due to its potential to increase plan quality in terms of reduced doses to normal tissue compared to conventional proton treatments delivered from a few static beams. The developments within the area have mostly been centered around delivery in a *dynamic mode*, that is, the protons are delivered while rotating the gantry (or alternatively the patient), in order to decrease treatment times and thus increase patient throughput. To enable dynamic arc delivery, much of the research efforts on the treatment planning side have been channeled to finding methods for assigning energy layers and spots over the continuous arc and improving the optimizing process in this setting.[1–6] On the treatment machine side, development efforts are made to introduce necessary adoptions, and proof-of-concept deliveries have already been performed.[7] However, no treatment machine is yet able to deliver in dynamic arc mode in a clinical setting either with a rotating gantry or with a fixed beam combined with a rotating chair. Moreover, the delivery during rotation introduces additional dosimetric uncertainty, which needs to be investigated in detail before clinical translation.

An alternative approach to dynamic arcs is to use *discrete arcs* (also denoted as *static arcs*), where step-and-shoot delivery is used over a large number of discrete directions with multiple energy layers per direction. A major advantage of this method is that these plans can be delivered as conventional intensity-modulated proton therapy (IMPT) plans, which means that they can be delivered using all existing treatment machines that support IMPT. With the step-and-shoot approach the dosimetric uncertainty introduced by rotation during delivery also disappears. Battinelli et al.[8] introduced a method for discrete proton arc optimization based on additive and subtractive greedy approaches for selection of energy layers from the discrete directions. When this method was employed to 10 oropharyngeal cancer patients, it was found that 360 layers distributed over 30 directions produced near optimal plans with reduced toxicity to normal tissue.[9,10] The disadvantage of this method is that a large number of beams will lead to very long and possibly even unacceptable treatment times, if introduced using conventional IMPT delivery. Technological advances, such as automatic sequencing of consecutive IMPT beams or delivery as a single step-and-shoot arc beam with no additional time between discrete directions other than the rotational time, could remove part of this problem. This step would still require both hardware and software development from the treatment machine vendors, as well as upgrades at the clinics.

In treatment planning studies proton arcs have shown potential benefits with respect to reduced organ-at-risk (OAR) doses,[9,11–17] reduced normal tissue complication (NTCP),[9,10] improved LET distributions,[18–20] and consequently improved variable radiobiological effective (RBE) dose distributions compared to IMPT.[21] More recently, there have been indications that proton arc treatments on the other hand could suffer from worse interfractional target robustness compared to conventional IMPT, as has been seen in studies for head and neck cancer patients.[22,23] One major reason in those cases could be that the proton arc treatments are delivered over many interlaced directions, compared to IMPT plans with a few beams and stacked energy layers. Proton arc treatments over a full revolution could also pass regions that are problematic from a robustness perspective, such as the shoulder areas. These regions are in general avoided in IMPT planning.[24] Moreover, to facilitate faster delivery and achieve more conformal dose distributions range shifters are omitted in proton arc plans, which results in more tangential incidence angles of the protons. Tangential beams are more sensitive to small changes in the patient surface compared to beams with more orthogonal incidence angles.

We propose a new method to partition the discrete arc plans into subplans, each subplan containing a subset of the directions. Each subplan is optimized to deliver a uniform dose in the target and one subplan is planned to be delivered per fraction. As an example, a discrete arc with 30 directions can be partitioned into 3 subplans with 10 directions each. The primary goal of the partitioning approach is to introduce a concept that keeps the advantages of discrete proton arc optimization in terms of previously reported plan quality improvements, while reducing treatment times to acceptable levels. Additionally, the approach of delivering uniform doses

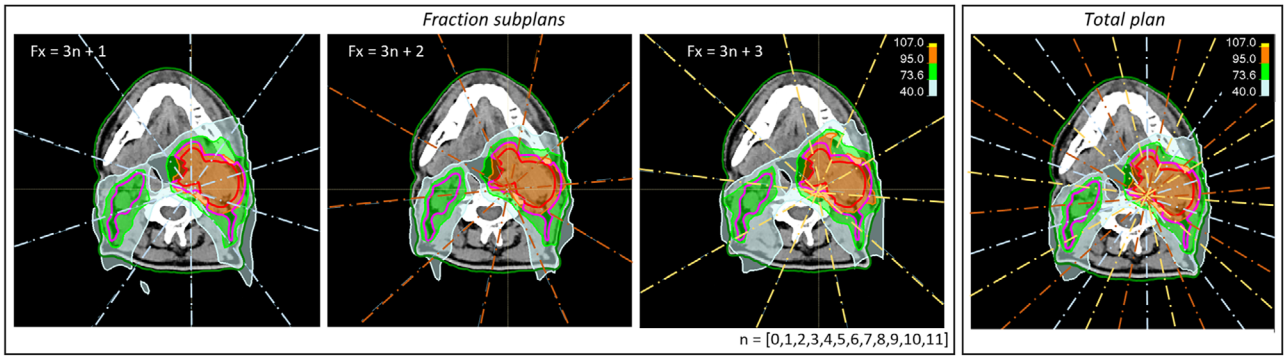

FIGURE 1 Example of a discrete arc plan partitioned into three interlaced subplans, each using 10 discrete directions (3×10). Each subplan is delivered every third fraction over in total 35 fractions. The first and second subplans are delivered in 12 fractions, while the last subplan is delivered in 11 fractions. The fourth panel shows the total plan with dose. The color table is given in percentage of the prescribed fraction dose (left panels) or total dose (right panel).

from different directions in alternating fractions has similarities to single-field uniform dose (SFUD) planning,[25] a heuristic method that was designed to increase the robustness of proton plans. The hypothesis is that partitioning of discrete arcs could overcome some of the problems with interfractional robustness.

2 | METHODS

2.1 | Patients and treatment planning

Three oropharyngeal cancer patients, which were previously treated with four- or five-beam IMPT plans in 35 fractions, were chosen for this study. Two of the IMPT beams used range shifters for part of the beams in order to treat the shallow volumes of the tumor. All patients had two distinct target volumes (CTV7000 and CTV5425) with prescription levels of 70 Gy_{RBE} and 54.25 Gy_{RBE} over the full treatment. The target volumes were on average 91 and 333 cm^3, respectively. At time of treatment, weekly repeated CTs were acquired for each of the patients.

For each of the patients we initially created three discrete arc plans, all planned with 360 energy layers over 30 directions in total spread over a full revolution. One plan delivers all directions in every fraction, while the other plans are partitioned into subplans with 10 and 6 directions:

- **1×30**: 1 plan with 30 directions and 360 layers per fraction.
- **3×10**: 3 subplans, each with 10 directions and 120 energy layers per fraction. Each subplan is delivered every 3rd fraction. (Figure 1 gives an example of the 3×10 plan for one of the patients.)
- **5×6**: 5 subplans, each with 6 directions and 72 energy layers per fraction. Each subplan is delivered every 5th fraction.

In addition to the three plans with the same number of total directions, we created a plan with 10 directions per fraction but in total 70 directions:

- **7×10**: 7 subplans, each with 10 directions and 120 energy layers per fraction. Each subplan is delivered every 7th fraction. The resulting plan should in principle be similar in delivery time as the 3×10 plan, but with additional degrees of freedom in the optimization.

As for the clinical IMPT plan, we have used a machine model of an IBA Proteus Plus system, which is a multi-room system with the capability to rotate the gantry from −180° to 180°. All discrete arc plans were planned in a pre-release version of RayStation 2023B, which has support for discrete arc planning through an energy layer filtering (ELF) approach. This approach is similar, but not identical to the energy layer reduction (ELR) technique.[8,9] In ELF the arc is set up by a start and stop gantry angle, a number of irradiation directions, an initial and final number of energy layers. Throughout the optimization, the lowest weighted energy layers are filtered out to reach the final number of energy layers. After the energy layer filtering steps, low-weighted spots are filtered out to respect the minimum spot MU limit of the machine (0.011 MU in this case).

In the arc plans for this study, no range shifter has been used in order to remove the need for snout position adjustments and thereby facilitate a faster change between beams. The arc plans were, like the clinical IMPT plans, all optimized with robust constraints on the targets using 3% range and 3 mm setup uncertainties. A constant radiobiological effectiveness (RBE) factor of 1.1 was used for all treatment plans. For the plans that were split into subplans (3×10, 5×6, and 7×10), the optimizer was constrained to respect the minimum and maximum target constraints in every fraction, while the objectives for the OARs were set over the full treatment to keep the flexibility of the total number of directions.

To achieve this in practice, the partitioned plans were initially set up with 3, 5, and 7 discrete arc beams, respectively. All beams were optimized simultaneously using beam-specific constraints for the targets, while OAR objectives related to the full plan. The splitting into subplans was performed as a scripted post-processing step, in which each initial arc beam was distributed to a dedicated subplan. Since all directions are optimized simultaneously regardless of the type of arc plan, the optimization times are comparable for the partitioned and non-partitioned arc plans.

2.2 | Delivery time estimate

For the delivery time estimate, we have used a simple time model to estimate the irradiation of energy layers with spots from the discrete directions, as well as the rotation time between the discrete directions. This corresponds to the delivery time for one single arc beam in step-and-shoot mode, that is, all directions are delivered without any interruption between beams beyond gantry motion. Additionally, we assess the delivery time as if it consisted of many IMPT beams. In terms of delivery, this will introduce extra time between beams for manual interactions with the treatment delivery software. We have simulated this additional time by adding 10, 20, or 30 s between the separate beams/directions.

The time model uses typical mechanical parameters from an IBA Proteus One system[4] with a rotational speed of 6°/s and acceleration of 0.6°/s^2. Spot irradiation times were inferred from Pfeiler et al.[26] A constant time of 2 ms to switch between spots was employed irrespective of the distance between the spots. The upward switching time between energy layers was set to 6 s and the downward switching time to 0.8 s. In addition to the switching times, a dead time of 0.3 s before start of irradiation of an energy layer is simulated.

The same delivery time estimate method was used for the arc plans and the IMPT plans. Note that the IMPT plans employ range shifters for two of the beams, which in current clinical settings would require additional time in-between beams to avoid collisions when the snout position is changed to reduce the air gap between range shifter and patient. The reported delivery times for the IMPT plans should therefore be seen as a lower estimate.

2.3 | Scenario-based dose accumulation

To assess the plan robustness with respect to changes in the patient geometry as well as to setup and range errors over the full treatment course, a detailed robustness evaluation is made through construction of accumulated scenario doses in each fraction. For the planning CT (pCT) and each of the weekly repeated CTs (rCTs), 30 fraction scenarios are computed with range uncertainties of ±3% for the nominal position, as well as for position uncertainties of 3 mm in 14 directions (six points along the main axes and eight points along the diagonals.)

We assume that the same systematic error is present in each fraction and can thus accumulate the scenario doses with the same uncertainties over the delivered fractions. This results in 30 treatment scenarios consisting of accumulated doses over multiple fractions. The fraction scenario dose in a specific fraction is approximated by the scenario dose computed on the most recently acquired CT. As an example, if the first two rCTs are taken at fractions 4 and 9, the pCT is used for fractions 1–3, the first rCT is used for fractions 4–8, and the second rCT is used from fraction 9 until the fraction for the third rCT. The principle is illustrated in Figure 2 when there is only one subplan. In this case the fraction scenario doses are the same in fractions with the same CT. When multiple subplans are used, 30 scenarios are computed per CT and per subplan. In the creation of an accumulated fraction scenario dose $D_S{}^n$ for scenario S and fraction n, the correct subplan dose on the corresponding CT, $d_S{}^{\mathrm{CT}n,\mathrm{SP}n}$, is used in each fraction according to the treatment course schedule:

$$D_S^n = D_S^{n-1} + d_S^{\mathrm{CT}n,\mathrm{SP}n} \tag{1}$$

where CT_n and SP_n are the CT and the subplan in fraction n, respectively.

As an example, when there are three subplans and the first rCT is acquired in fraction four, the first four accumulated scenario doses for uncertainty scenario 1 will read

$$\mathrm{Fx1} : D_1^1 = d_1^{\mathrm{pCT,SP1}}$$

$$\mathrm{Fx2} : D_1^2 = D_1^1 + d_1^{\mathrm{pCT,SP2}}$$

$$\mathrm{Fx3} : D_1{}^3 = D_1{}^2 + d_1^{\mathrm{pCT,SP3}}$$

$$\mathrm{Fx4} : D_1^4 = D_1^3 + d_1^{\mathrm{rCT1*,SP1}}$$

The star (*) in $d_1{}^{\mathrm{rCT1*,\,SP1}}$ denotes that the dose on rCT_1 has been mapped to pCT in order to be able to perform dose accumulation.

2.4 | Target robustness evaluation

The robustness with respect to target coverage is assessed using the voxel-wise minimum dose approach.[27] For each of the fractions the voxel-wise minimum of the accumulated physical dose is equated. The volume at 95% of the prescribed accumulated fraction dose (V95%) is assessed for the CTV7000 and the CTV5425.

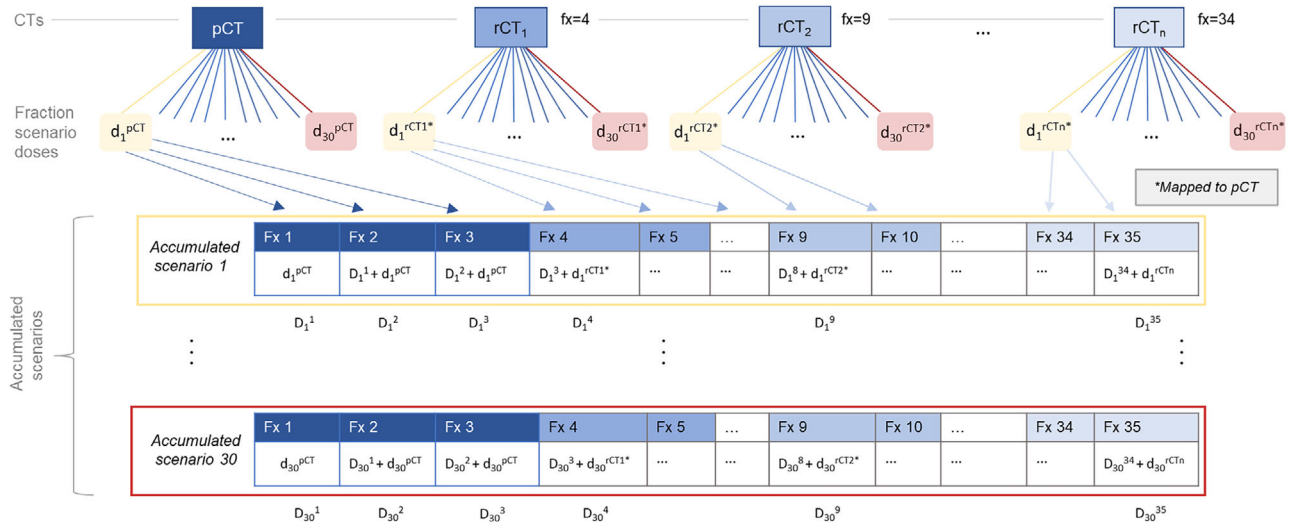

FIGURE 2 Principles of scenario-based dose accumulation for a plan without beam partitioning (only one subplan). The most recently taken CT is used in each fraction and 30 robustness evaluation scenarios are computed on each CT. The doses on the rCTs are mapped to the pCT. The same systematic range and setup errors are assumed in each fraction making it possible to accumulate scenario doses with the same errors over all 35 fractions. The result is a set of 30 accumulated scenario doses in each fraction.

2.5 | OAR dose and NTCP evaluation

For the OARs, we use the worst value of the clinical goal evaluated over all accumulated scenario doses in fraction 35. Using this metric, we assess the body integral dose (ID),[9] the volume of the body at 1 and 3 Gy_{RBE} ($V1Gy_{RBE}$ and $V3Gy_{RBE}$), the dose at 1% volume (D1%) to the spinal cord and the brainstem, as well as the mean dose (D_{mean}) to the parotids, submandibular glands, and the oral cavity.

NTCP for xerostomia and dysphagia is evaluated in each fraction for each accumulated scenario dose using the models from the Dutch model-based approach.[28] The accumulated fraction dose is extrapolated to a total treatment course dose in order to be able to assess the NTCP in each fraction. The extrapolation is performed by multiplying the accumulated fraction dose with the quotient between the total number of fractions and the delivered number of fractions. We equate the ΔNTCP between the arc plans and the IMPT plan in every scenario and investigate the mean value and standard deviation of ΔNTCP over all scenarios.

For both the OAR dose and NTCP evaluation, a biologically equivalent dose is used to account for spreading the dose in normal tissue differently over fractions.

2.6 | Biologically equivalent dose

The biologically equivalent accumulated fraction dose in fraction n and voxel j, $D_{n,j}^{EQD}$, is computed using the linear-quadratic model:

$$D_{n,j}^{EQD} = n\left(\sqrt{\frac{\alpha^2}{4\beta^2} + \frac{1}{n}\sum_{i=1}^{n}\left(\frac{\alpha}{\beta}d_{i,j} + d_{i,j}^2\right)} - \frac{\alpha}{2\beta}\right) \quad (2)$$

where $d_{i,j}$ is the mapped scenario dose on the pCT in voxel j in fraction i taking the corresponding CT and subplan into account.

For the normal tissue, we employ a constant α/β-ratio of 3. Even if there could be a substantial delay between the deliveries of the same subplans for some of the plans, any potential repair between fractions is omitted for simplicity. This follows the same principle as outlined by Bortfeld et al.[29] The biologically equivalent dose concept is only used for the normal tissue and not for the tumor, since the dose to the tumor is constrained to be uniform in the target over the fractions meaning that the variations are small. Additionally, tumors have in general a higher α/β, which puts it closer to the physical dose.

3 | RESULTS

3.1 | Delivery time

As can be seen in Figure 3, the delivery time has a strong dependence on the number of beams in each subplan to be delivered. With 30 beams the continuous delivery over different directions in one step-and-shoot beam is just above 10 min. However, when adding time between

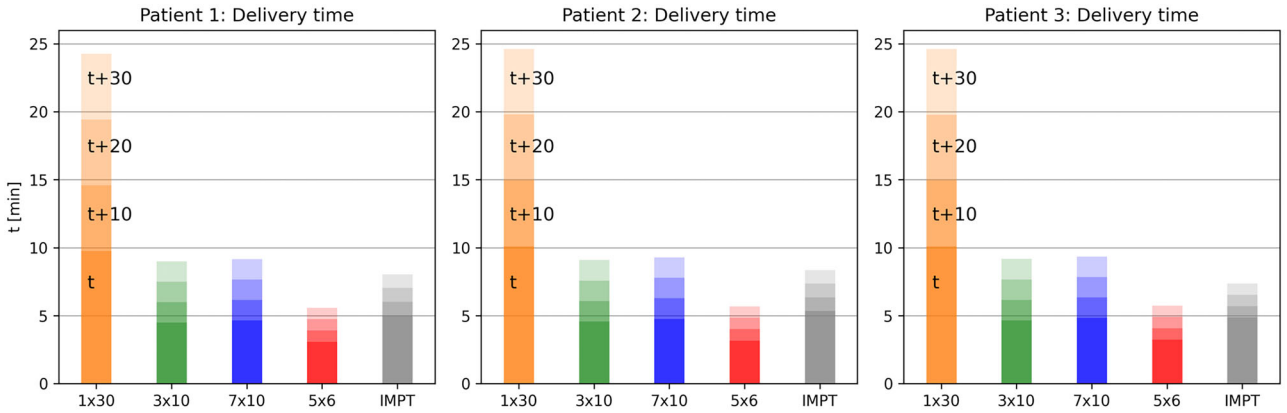

FIGURE 3 Delivery times for the three patients for the five different plans. For plans with several subplans the mean values are presented. In all cases the variation between the different subplans is small (standard deviation below 1 s). The lowest solid bar (t) represents continuous delivery over different directions in one step-and-shoot beam, including the time for rotating the gantry between the discrete directions. The additional bars (with increasing transparency) represent additions of 10, 20, and 30 s ($t + 10$, $t + 20$, $t + 30$) for manual interactions with the treatment software in between beams.

beams the total delivery time increases dramatically to around 15, 20, and 25 min with delays of 10, 20, and 30 s, respectively. The fastest plans to deliver are without doubt the 5×6 arcs with mean delivery times ranging between around 3.2 min (no delay) and 5.7 min (30 s delay). The plans with 10 directions in each subplan are comparable in total delivery time to the IMPT plans, when the delays between beams are moderate (≤20 s). The estimated delivery time for the arc subplans with 10 directions is well below 10 min when 30 s delay is employed and around 5 min when no delay is added between beams.

The number of spots per fraction is comparable between the IMPT plans and the 3×10 plans, but the number of energy layers per fraction is 56%–82% higher for the IMPT plan. This difference explains why the delivery times without additional time are shorter for the 3×10 plan than for the IMPT plans, even though the 3×10 plans have at least the double number of directions. Similar numbers are seen for the 7×10 plans, while the 5×6 plans have both substantially lower number of spots and energy layers. (See Table S1 in the Supplementary material for more information.)

3.2 | Target robustness

Figure 4 displays the target robustness evaluated as the V95% of the voxel-wise minimum over the accumulated scenarios in each fraction for both CTV7000 and CTV5425.

In general, the target robustness is best for the 5×6 plans, followed by the plans with 10 directions (3×10 and 7×10). The 1×30 plan performs worst among the arc plans. The IMPT plan is in all cases superior to the 1×30 plan with respect to target coverage, whereas the partitioned arc plans in many cases perform better than the IMPT plan, with the exception of the CTV7000 for patient 3.

It can be clearly seen that the first fractions for the partitioned plans are less robust than the non-partitioned plans. The effect of increased robustness comes after a few fractions, when the accumulation of uniform doses from different directions comes into play.

3.3 | OAR metrics

For the doses to OARs, Figure 5a displays the relative biologically equivalent worst-case accumulated doses at fraction 35 relative to the 1×30 plan. In Figure 5b, the absolute values in biologically equivalent worst-case accumulated doses are given together with the difference in percent to the corresponding physical dose. Some of the smaller structures, such as the spinal cord and the brainstem, show substantial differences to the corresponding physical dose indicating the need for evaluation using biologically equivalent doses. For the arc plans, the doses are in general best for the 1×30 plan, followed closely by the 7×10 and 3×10 plans. The 5×6 plan is inferior to the other arc plans and for several OARs also compared to the IMPT plan.

There is a notable inter-patient variability and no overall trend over patients can be seen. One specific example is the low-dose envelope (measured in V1Gy and V3Gy), which varies between patients with two of the patients having lower values for the reference arc plan compared to the IMPT plan, while one patient shows an increased low-dose envelope for the arc plans.

3.4 | NTCP evaluation

Figure 6 shows mean ΔNTCP values for xerostomia and dysphagia (grade ≥2) between each arc plan and the

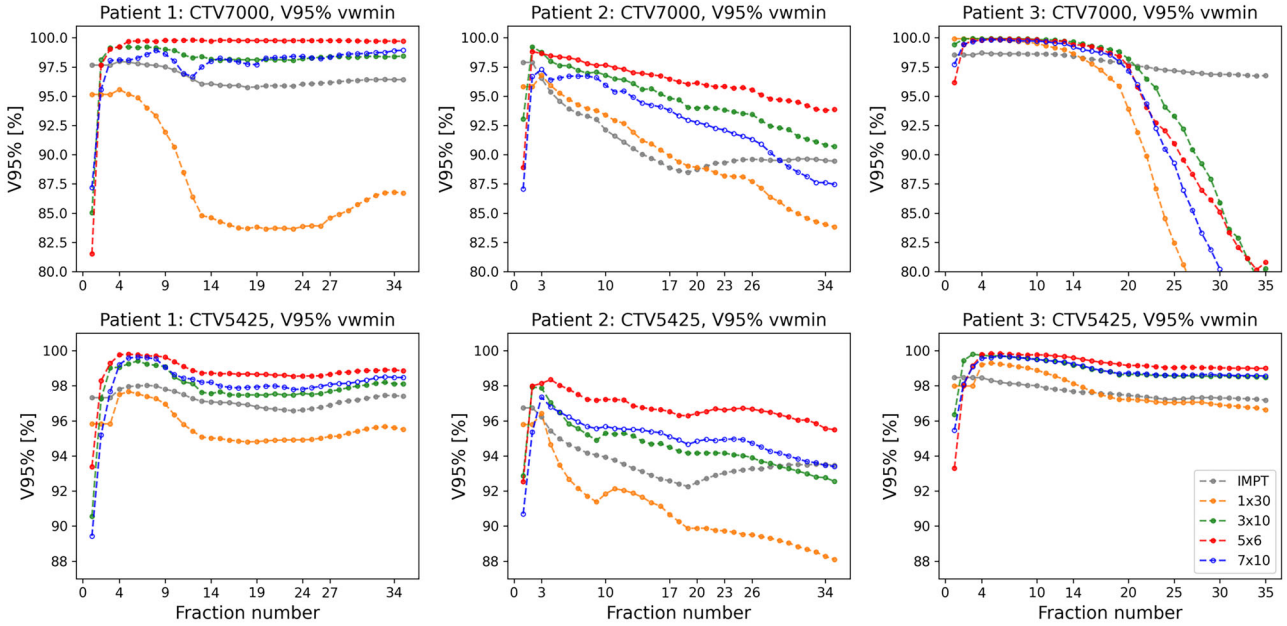

FIGURE 4 Target robustness over all fractions for CTV7000 (upper panel) and CTV5425 (lower panel). For each CT (pCT and rCTs), 30 robustness evaluation scenarios based on 3% range and 3 mm setup uncertainty have been computed. Scenario doses have subsequently been accumulated over fractions and the voxel-wise minimum dose distribution is computed based on the accumulated scenario doses in each fraction. The volume at 95% of the prescribed dose of the voxel-wise minimum dose distribution over the accumulated scenarios has been evaluated. Displayed fraction numbers on the *x*-axes correspond to fractions where a CT has been taken.

IMPT plan. It can be noted that the 1×30, 7×10, and 3×10 plans all offer NTCP reductions for all patients up to a few percentage points (p.p.), except for xerostomia for patient 2. For the 5×6 plans, the NTCP is similar or worse compared to the clinical IMPT plans. It can also be seen that the NTCP reduction for dysphagia for two of the patients clearly diminishes over the treatment course.

Xerostomia and dysphagia of grade ≥3 follow the same trends over the treatment course as the grade ≥2 counterparts displayed in Figure 6, but at lower values. When comparing the different plans in the beginning of the treatment (at fraction 5), the largest reduction in NTCP is seen for dysphagia grade ≥2 for patient 2 for the 1×30 plan with a value of -4.8 ± 1.6 p.p. The corresponding values for the 3×10 and 7×10 plans are -2.6 ± 1.6 p.p. and -3.3 ± 1.9, respectively. At the last fraction, these reductions have all become smaller by 1.5–1.7 p.p. In general, the variation in ΔNTCP over the different scenarios is moderate with a standard deviation below 0.3 p.p. in most cases. However, for some cases the standard deviation can reach as high as 1.9 p.p. (See Table S2 in the Supplementary material for more information.)

4 | DISCUSSION

We have presented a method for partitioning discrete arc plans into subplans with a subset of the total number of directions in each subplan. The subplans are delivered interlaced in adjacent fractions. This results in highly reduced delivery times. Additionally, all partitioned arc plans in this study show better robustness over the treatment course than the standard arc plans. We see that the partitioning of the arc plans reduces some of the OAR sparing effect and for the highly partitioned 5×6 plans it has completely disappeared. For the studied partitioning setups, the optimal choice with respect to delivery time, target robustness and OAR sparing is to use 10 directions. The limiting factor for the delivery time is the number of directions and energy layers with spots delivered in each fraction. By increasing the number of total directions in the plan from 30 (3×10) to 70 (7×10) while keeping the number of directions and energy layers per fraction constant, the delivery time stays at the same level at the same time as the optimizer is given more freedom. This results in some cases in slightly reduced OAR doses and NTCP values.

The delivery time estimate given in this study is based on a simple time model of an IBA Proteus Plus machine, and the reported times are given for continuous delivery over different directions in one step-and-shoot beam, as well as for standard IMPT delivery with simulated manual interventions between the beams. The delivery times will be dependent on the treatment machine, but for all machines beam partitioning will reduce treatment times and could thus pave the way for inclusion of high-quality proton arc plans at existing proton beam facilities without any replacement of hardware. It could also be a viable option to introduce arc delivery at light

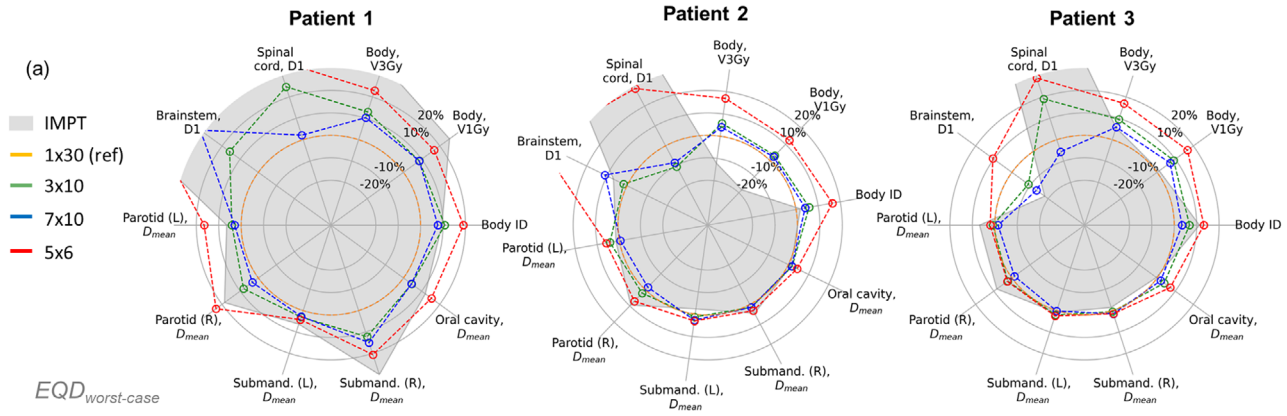

(b)

	Patient 1					Patient 2					Patient 3				
	IMPT	1x30	3x10	7x10	5x6	IMPT	1x30	3x10	7x10	5x6	IMPT	1x30	3x10	7x10	5x6
Body,	75.7	69.1	76.6	74.4	82.3	90.0	88.3	93.5	91.9	102.8	102.0	91.7	98.0	94.9	103.9
ID [Gy(RBE)·l]	(0.2)	(0.2)	(1.9)	(1.7)	(3.6)	(0.6)	(0.5)	(1.9)	(2.1)	(4.1)	(0.2)	(0.3)	(1.2)	(1.3)	(2.9)
Body,	31.9	25.4	27.6	27.6	29.7	25.1	30.7	31.6	31.4	34.5	32.2	31.8	34.7	34.1	37.1
V1Gy [%]	(0.3)	(0.2)	(2.1)	(2.1)	(3.4)	(0.5)	(0.5)	(2.2)	(2.5)	(3.5)	(0.2)	(0.2)	(1.5)	(1.7)	(3.5)
Body,	27.0	20.0	22.6	22.0	24.6	21.9	24.9	26.3	25.9	29.1	27.8	26.3	28.8	27.9	30.8
V3Gy [%]	(0.4)	(0.3)	(2.9)	(3.0)	(5.4)	(0.6)	(0.6)	(3.5)	(4.0)	(6.2)	(0.3)	(0.3)	(2.2)	(2.3)	(4.4)
Spinal cord,	44.0	12.6	15.7	12.9	17.3	35.8	9.8	8.7	8.9	12.6	33.4	11.2	13.4	10.6	14.4
D1% [Gy(RBE)]	(0.0)	(1.7)	(5.2)	(9.4)	(7.1)	(0.0)	(1.6)	(2.4)	(6.3)	(5.6)	(0.0)	(1.2)	(1.8)	(3.0)	(5.9)
Brainstem,	11.2	3.8	4.4	5.0	6.6	4.4	4.1	4.2	4.6	5.9	9.0	10.9	9.9	9.4	12.1
D1% [Gy(RBE)]	(0.0)	(0.1)	(10.5)	(8.4)	(9.7)	(0.5)	(2.0)	(22.9)	(21.6)	(33.6)	(0.0)	(0.0)	(0.4)	(4.5)	(5.9)
Parotid (L),	25.6	24.0	25.0	24.7	28.0	19.7	19.4	20.2	19.3	20.5	37.6	35.2	35.5	34.7	35.9
D_{mean} [Gy(RBE)]	(0.1)	(0.2)	(0.5)	(0.5)	(1.4)	(0.4)	(0.7)	(1.2)	(1.5)	(1.6)	(0.1)	(0.1)	(0.4)	(0.4)	(0.8)
Parotid (R),	9.6	8.1	8.7	8.4	10.0	18.0	16.4	16.8	16.2	17.6	22.7	20.9	21.4	20.6	21.5
D_{mean} [Gy(RBE)]	(0.3)	(0.5)	(1.6)	(1.7)	(3.6)	(1.0)	(0.9)	(1.4)	(1.8)	(1.9)	(0.2)	(0.3)	(1.3)	(1.4)	(2.1)
Submand. (L),	68.2	64.2	66.1	65.9	66.8	55.5	56.9	57.6	58.4	58.6	54.8	54.3	55.4	54.4	55.7
D_{mean} [Gy(RBE)]	(0.0)	(0.0)	(0.1)	(0.1)	(0.1)	(0.0)	(0.1)	(0.2)	(0.3)	(0.5)	(0.1)	(0.1)	(0.2)	(0.3)	(0.5)
Submand. (R),	30.5	23.5	26.4	27.0	28.3	66.7	63.9	64.8	64.8	65.9	43.4	44.1	44.3	44.7	44.7
D_{mean} [Gy(RBE)]	(0.4)	(0.3)	(1.4)	(1.9)	(2.6)	(0.0)	(0.0)	(0.1)	(0.1)	(0.1)	(0.2)	(0.3)	(0.7)	(0.9)	(1.5)
Oral cavity,	24.6	22.0	23.0	23.0	25.4	54.8	54.1	55.1	55.0	56.5	24.6	24.7	25.6	25.2	26.5
D_{mean} [Gy(RBE)]	(0.7)	(0.4)	(2.0)	(1.7)	(3.3)	(0.2)	(0.3)	(0.5)	(0.5)	(0.6)	(0.3)	(0.4)	(1.1)	(1.2)	(1.8)

FIGURE 5 (a) Spider plots for relative differences of the worst-case accumulated doses to OARs for the different plans at fraction 35 compared to the corresponding worst-case accumulated doses of the 1×30 plan. All doses are equated as biologically equivalent doses (EQD). (b) Table with the corresponding absolute values of biologically equivalent doses for the OARs for the different plans. The values in parentheses show the difference in percent to the corresponding physical dose: $\Delta D = (D_{EQD} - D_{PHY}) / D_{EQD}$.

ion facilities. Light ion arcs with single or multi-ions could substantially reduce dose to normal tissue as well as focus high LET into the target.[30,31] However, there are still challenges on the delivery side, which could be remedied by partitioned discrete ion arcs. In a multi-ion setting, the method could potentially be adopted to use different ions in different fractions.

Advances made for dynamic proton arc delivery[7] could be used to deliver non-partitioned discrete arc plans more efficiently (around 10 min for the three oropharyngeal cancer patients in this study). However, the beam partitioning approach would also in a continuous delivery mode substantially reduce the total treatment time. (In this exploratory study the gain was around a factor of two or more). Both for standard IMPT and continuous delivery, the administration of the delivery would be facilitated by improved system support in the oncology information system for delivery of different subplans in different fractions.

The interfractional robustness was improved for the partitioned plans in this study, in line with the hypothesis based on the similarities to SFUD planning. The individual beam sets do not show to be more robust when recomputed on the rCTs. It is instead the combination of homogeneous target doses from different directions that makes the partitioned plans less sensitive to changes in the patient anatomy. Beam partitioning could therefore reduce the need for adaptive replanning of proton arc plans. Nevertheless, in some cases, the partitioned arc plans will still be less robust than a traditional IMPT plan, possibly due to the presence of more tangential incidence angles in the arc plans and irradiation from many different directions, including those that are less beneficial from a robustness

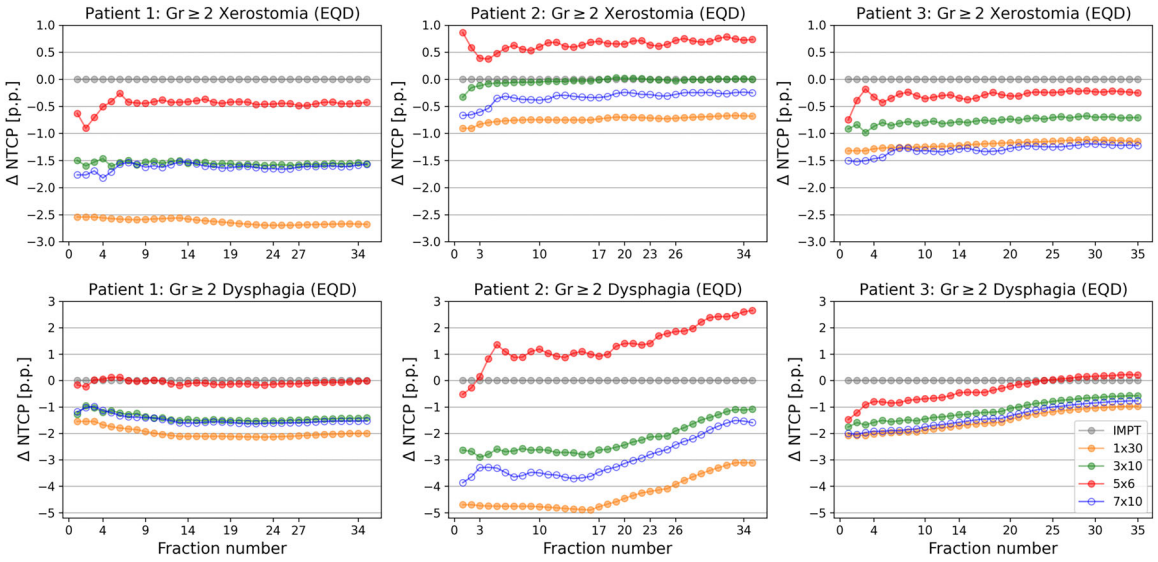

FIGURE 6 Mean ΔNTCP values for grade ≥2 xerostomia and dysphagia over the 35 fractions in the treatment course. The ΔNTCP is computed as the difference in NTCP between each arc plan and the IMPT plan for each systematic accumulated scenario, S, ($\Delta\text{NTCP} = \text{NTCP}_S^{\text{Arc}} - \text{NTCP}_S^{\text{IMPT}}$) and the mean value is equated over all 30 scenarios. The NTCP estimation is based on the biologically equivalent accumulated dose. Displayed fraction numbers on the x-axes correspond to fractions where a CT has been taken.

perspective. For patient 3, the robust target coverage of the CTV7000 is not satisfactory for the arc plans over the treatment course and here adaptive replanning would be needed in a clinical setting. For this patient, there were large changes in the patient anatomy over the treatment course: the CTV7000 volume of 135 cm^3 in the planning CT decreased by at most 19 cm^3 (in rCT20) and the corresponding movement of the patient surface was around 7 mm. This is substantially larger than what is accounted for in robust optimization. Based on these findings, it will therefore be important to make a thorough assessment of the target robustness throughout the treatment course of all types of arc plans, regardless of whether beam partitioning has been used or not. OAR doses should also be monitored and adaptive replanning considered in case of OAR dose deviations, since Figure 6 indicates that NTCP can get worse over the treatment course.

The method of beam partitioning could also be used for dynamic arcs. There could be a major gain in delivery time by reducing the number of energy layers per fraction, which would enable faster continuous movement of the gantry. Moreover, the interfractional robustness should be improved by the same principles as for discrete arcs. Since the delivery of a dynamic arc plan is expected to be faster than a discrete arc plan with many directions, the user could even choose to deliver the full plan, that is, all subplans, in every fraction. This would instead result in longer delivery times, but there would be less concerns about the biologically equivalent dose, when the same dose distribution is delivered in all fractions, as well as less complex administrations of plans when the same plan is delivered every fraction.

From a patient-specific quality assurance (PSQA) perspective, discrete arc plans pose less challenges than dynamic arc plans, where the dose is delivered during rotation. Nevertheless, the high number of beams in a discrete arc plan would require additional burden in PSQA, if each beam is to be verified separately. Necessary developments in PSQA for dynamic arc plans, such as gantry-mounted measurement devices, and the use of secondary dose calculation based on log files[32] will be useful approaches also for discrete arc delivery.

Biologically equivalent doses must in general be accounted for when distributing doses differently over different fractions. In fact, due to the changing patient geometry throughout the treatment course, there will also be an effect for the plans with only one subplan (IMPT and 1×30), but it is much smaller than for the beam partitioned plans. We have employed a simplified model for biologically equivalent dose computation based on the linear-quadratic model with a constant α/β-ratio of 3 for all OARs. The model introduces per se extra uncertainty, and the effect should be further investigated in future studies both with a higher variability in α/β in simulation studies as well as in follow-up clinical trials. Smolders et al.[33] retrospectively accounted for the biologically equivalent dose for inter- and intra-fractional 4D dose accumulation in regular proton plans for lung cancer treatments using a set of different α/β-ratios. They concluded that while the translation from physical to biologically equivalent dose had an effect, the dose accumulation in the studied cases was affected more by uncertainties in the deformable image registration than in the variations in α/β ratio. More complex models introducing time effects[34] could also be

considered. With possible repair within the treatment course the biologically effective dose might get closer to the physical dose.

In our study, the method of scenario-based dose accumulation has given valuable information of the changes over the treatment course of the target robustness, as well as OAR doses and NTCP values. As was seen in Figures 4 and 6, the variability over the treatment course is large with in general decreasing target robustness and decreasing NTCP reductions with increasing fractions. A potential large reduction in NTCP seen in treatment planning before the treatment starts might thus not be fully retained throughout the treatment.

This study should be seen as a proof-of-concept for the beam partitioning approach. Future research should include a larger patient cohort since the inter-patient variability can be high. Given this high variability, the optimization objectives could be tailored to each patient in order to find the right balance between target robustness and normal tissue sparing. With less strict uniform target objectives, the NTCP values compared to IMPT could probably be reduced further. It could be noted that the reported NTCP reductions in this study are in general lower than previous proton arc studies for oropharyngeal cancer patients.[9,10] We, therefore, see room for improvement in the reported NTCP reductions when assessing the results over a larger patient cohort and with more tailored optimization objectives. The increased degrees of freedom in the arc plans (both partitioned and non-partitioned) could be utilized to reduce high LET in OARs, if combined with robust LET optimization objectives.[20] Since the subplans are delivered in different fractions, a change in the couch angle could be applied between the different subplans without losing any time in delivery. This could be used both for dynamic and discrete arcs in cases where it would be beneficial with a full arc, but the plan is delivered by a compact gantry that only supports a limited gantry angle range, such as the IBA Proteus One system. Additionally, it would allow for non-coplanar beams for the full treatment plan and could introduce larger room for sparing normal tissue. A similar technique has been employed in combination with beam angle optimization for photon IMRT.[35] Our approach could be extended to coplanar or non-coplanar IMRT and VMAT treatments and would have the advantage of applying pre-defined beams or arcs, removing the need for time-consuming beam angle optimization.

5 | CONCLUSIONS

Partitioning of discrete proton arcs can be used to highly reduce delivery times, when there is a large number of total discrete directions. The approach also improves interfractional target robustness. For the studied oropharyngeal cancer patients and the tested plans, 10 beam directions per fractions is the preferred choice. The doses to OARs and NTCP values for these plans are close to the non-partitioned arc plans with 30 directions and thereby superior to the IMPT plans, while the treatment times can be reduced by almost a factor of three compared to the non-partitioned arc plans.

This work paves the way towards utilizing the benefits of arc treatments by delivering those plans as conventional IMPT plans in existing proton and light-ion facilities. With the advent of hardware development for delivery in arc mode, the new technique can be used to further reduce treatment times and improve interfractional robustness.

ACKNOWLEDGMENTS

Jakob Ödén is acknowledged for fruitful discussions on biologically equivalent doses.

CONFLICT OF INTEREST STATEMENT

The authors from RaySearch Laboratories are all employees of the company. University Medical Center Groningen has research contracts with Ion Beam Applications (IBA), Louvain-La-Neuve, Belgium and RaySearch Laboratories.

REFERENCES

1. Sanchez-Parcerisa D, Kirk M, Fager M, et al. Range optimization for mono- and bi-energetic proton modulated arc therapy with pencil beam scanning. *Phys Med Biol*. 2016;61(21):N565-N574. doi:10.1088/0031-9155/61/21/N565
2. Ding X, Li X, Zhang JM, Kabolizadeh P, Stevens C, Yan D. Spot-scanning proton arc (SPArc) therapy: the first Robust and delivery-efficient spot-scanning proton arc therapy. *Int J Radiat Oncol*. 2016;96(5):1107-1116. doi:10.1016/j.ijrobp.2016.08.049
3. Gu W, Ruan D, Lyu Q, Zou W, Dong L, Sheng K. A novel energy layer optimization framework for spot-scanning proton arc therapy. *Med Phys*. 2020;47(5):2072-2084. doi:10.1002/mp.14083
4. Liu G, Li X, Zhao L, et al. A novel energy sequence optimization algorithm for efficient spot-scanning proton arc (SPArc) treatment delivery. *Acta Oncol*. 2020;59(10):1178-1185. doi:10.1080/0284186X.2020.1765415
5. Engwall E, Battinelli C, Wase V, et al. Fast robust optimization of proton PBS arc therapy plans using early energy layer selection and spot assignment. *Phys Med Biol*. 2022;67(6):065010. doi:10.1088/1361-6560/ac55a6
6. Wuyckens S, Saint-Guillain M, Janssens G, et al. Treatment planning in arc proton therapy: comparison of several optimization problem statements and their corresponding solvers. *Comput Biol Med*. 2022;148:105609. doi:10.1016/j.compbiomed.2022.105609
7. Li X, Liu G, Janssens G, et al. The first prototype of spot-scanning proton arc treatment delivery. *Radiother Oncol*. 2019;137:130-136. doi:10.1016/j.radonc.2019.04.032
8. Battinelli C. Proton Arc Therapy Optimization. KTH, Optimization and Systems Theory. Master's Thesis; 2019.
9. de Jong BA, Battinelli C, Free J, et al. Spot scanning proton arc therapy reduces toxicity in oropharyngeal cancer patients. *Med Phys*. 2022; 50(3):1305-1317. doi:10.1002/mp.16098. Published online October 2022.

10. de Jong BA, Korevaar EW, Maring A, et al. Proton arc therapy increases the benefit of proton therapy for oropharyngeal cancer patients in the model based clinic. *Radiother Oncol*. 2023;184:109670. doi:10.1016/j.radonc.2023.109670
11. Ding X, Li X, Qin A, et al. Have we reached proton beam therapy dosimetric limitations? – A novel robust, delivery-efficient and continuous spot-scanning proton arc (SPArc) therapy is to improve the dosimetric outcome in treating prostate cancer. *Acta Oncol*. 2018;57(3):435-437. doi:10.1080/0284186X.2017.1358463
12. Li X, Kabolizadeh P, Yan D, et al. Improve dosimetric outcome in stage III non-small-cell lung cancer treatment using spot-scanning proton arc (SPArc) therapy. *Radiat Oncol*. 2018;13(1):35. doi:10.1186/s13014-018-0981-6
13. Chang S, Liu G, Zhao L, et al. Feasibility study: spot-scanning proton arc therapy (SPArc) for left-sided whole breast radiotherapy. *Radiat Oncol*. 2020;15(1):232. doi:10.1186/s13014-020-01676-3
14. Ding X, Zhou J, Li X, et al. Improving dosimetric outcome for hippocampus and cochlea sparing whole brain radiotherapy using spot-scanning proton arc therapy. *Acta Oncol*. 2019;58(4):483-490. doi:10.1080/0284186X.2018.1555374
15. Liu G, Li X, Qin A, et al. Improve the dosimetric outcome in bilateral head and neck cancer (HNC) treatment using spot-scanning proton arc (SPArc) therapy: a feasibility study. *Radiat Oncol*. 2020;15(1):21. doi:10.1186/s13014-020-1476-9
16. Liu G, Li X, Qin A, et al. Is proton beam therapy ready for single fraction spine SBRS? – a feasibility study to use spot-scanning proton arc (SPArc) therapy to improve the robustness and dosimetric plan quality. *Acta Oncol*. 2021;60(5):653-657. doi:10.1080/0284186X.2021.1892183
17. Liu G, Zhao L, Qin A, et al. Lung stereotactic body radiotherapy (SBRT) using spot-scanning proton arc (SPArc) therapy: a feasibility study. *Front Oncol*. 2021;11:664455. doi:10.3389/fonc.2021.664455
18. Bertolet A, Carabe A. Proton monoenergetic arc therapy (PMAT) to enhance LETd within the target. *Phys Med Biol*. 2020;65(16):165006. doi:10.1088/1361-6560/ab9455
19. Li X, Ding X, Zheng W, et al. Linear energy transfer incorporated spot-scanning proton arc therapy optimization: a feasibility study. *Front Oncol*. 2021;11:698537. doi:10.3389/fonc.2021.698537
20. Glimelius L, Marthin O, Wase V, et al. Robust LET optimization of proton arcs can substantially reduce high LET in critical structures. ESTRO conference contribution, 2023.
21. Carabe A, Karagounis IV, Huynh K, et al. Radiobiological effectiveness difference of proton arc beams versus conventional proton and photon beams. *Phys Med Biol*. 2020;65(16):165002. doi:10.1088/1361-6560/ab9370
22. Marthin O, Wase V, Bokrantz R, et al. Robustness in proton arc treatments for head and neck cancer patients: impact of gantry angle spacing and number of revolutions. PTCOG conference contribution, 2022.
23. de Jong BA, Zhao L, Wase V, et al. Comparison of static and dynamic proton arc treatment planning algorithms in oropharyngeal cancer. ESTRO conference contribution, 2023.
24. Scandurra D, Meijer TWH, Free J, et al. Evaluation of robustly optimised intensity modulated proton therapy for nasopharyngealcarcinoma. *Radiother Oncol*. 2022;168:221-228. doi:10.1016/j.radonc.2022.01.043
25. Lomax T. Intensity modulated proton therapy. In: DeLaney TF, Kooy HM, eds. *Proton and Charged Particle Radiotherapy*. Lippincott Williams & Wilkins; 2008.
26. Pfeiler T, Bäumer C, Engwall E, Geismar D, Spaan B, Timmermann B. Experimental validation of a 4D dose calculation routine for pencil beam scanning proton therapy. *Z Für Med Phys*. 2018;28(2):121-133. doi:10.1016/j.zemedi.2017.07.005
27. Korevaar EW, Habraken SJM, Scandurra D, et al. Practical robustness evaluation in radiotherapy – a photon and proton-proof alternative to PTV-based plan evaluation. *Radiother Oncol*. 2019;141:267-274. doi:10.1016/j.radonc.2019.08.005
28. Langendijk JA, Hoogeman MS, Monshouwer R, Verheij M. Landelijk Indicatie Protocol Protonen Therapie (versie 2.2) HOOFD-HALSTU - MOREN; 2019. Accessed 29 March 2023. https://nvro.nl/publicaties/rapporten
29. Bortfeld T, Jokivarsi K, Goitein M, Kung J, Jiang SB. Effects of intra-fraction motion on IMRT dose delivery: statistical analysis and simulation. *Phys Med Biol*. 2002;47(13):2203-2220. doi:10.1088/0031-9155/47/13/302
30. Mein S, Tessonnier T, Kopp B, et al. Biological dose optimization for particle arc therapy using helium and carbon ions. *Int J Radiat Oncol Biol Phys*. 2022;114(2):334-348. doi:10.1016/j.ijrobp.2022.04.025
31. Mein S, Kopp B, Tessonnier T, et al. Spot-scanning hadron arc (SHArc) therapy: a proof of concept using single- and multi-ion strategies with helium, carbon, oxygen, and neon ions. *Med Phys*. 2022;49(9):6082-6097. doi:10.1002/mp.15800
32. Meijers A, Guterres Marmitt G, Ng Wei Siang K, et al. Feasibility of patient specific quality assurance for proton therapy based on independent dose calculation and predicted outcomes. *Radiother Oncol*. 2020;150:136-141. doi:10.1016/j.radonc.2020.06.027
33. Smolders A, Hengeveld AC, Both S, et al. Inter- and intrafractional 4D dose accumulation for evaluating ΔNTCP robustness in lung cancer. *Radiother Oncol*. 2023;182:109488. doi:10.1016/j.radonc.2023.109488
34. Fowler JF. The linear-quadratic formula and progress in fractionated radiotherapy. *Br J Radiol*. 1989;62(740):679-694. doi:10.1259/0007-1285-62-740-679
35. O'Connor D, Yu V, Nguyen D, Ruan D, Sheng K. Fraction-variant beam orientation optimization for non-coplanar IMRT. *Phys Med Biol*. 2018;63(4):045015. doi:10.1088/1361-6560/aaa94f

SUPPORTING INFORMATION

Additional supporting information can be found online in the Supporting Information section at the end of this article.

How to cite this article: Engwall E, Marthin O, Wase V, et al. Partitioning of discrete proton arcs into interlaced subplans can bring proton arc advances to existing proton facilities. *Med Phys*. 2023;50:5723–5733. https://doi.org/10.1002/mp.16617